

This work was written as part of one of the author's official duties as an Employee of the United States Government and is therefore a work of the United States Government. In accordance with 17 U.S.C. 105, no copyright protection is available for such works under U.S. Law.

Public Domain Mark 1.0

<https://creativecommons.org/publicdomain/mark/1.0/>

Access to this work was provided by the University of Maryland, Baltimore County (UMBC) ScholarWorks@UMBC digital repository on the Maryland Shared Open Access (MD-SOAR) platform.

Please provide feedback

Please support the ScholarWorks@UMBC repository by emailing scholarworks-group@umbc.edu and telling us what having access to this work means to you and why it's important to you. Thank you.

Laser-Driven Growth of Silver Nanoplates on p-Type GaAs Substrates and Their Surface-Enhanced Raman Scattering Activity

Yugang Sun* and Matthew Pelton

Center for Nanoscale Materials, Argonne National Laboratory, 9700 South Cass Avenue, Argonne, Illinois 60439

Received: January 21, 2009; Revised Manuscript Received: March 02, 2009

Contact between aqueous solutions of silver nitrate (AgNO_3) and pristine surfaces of p-type gallium arsenide (GaAs) wafers results in essentially no reaction at room temperature and in the dark. The galvanic reactions between the GaAs wafers and AgNO_3 can be triggered under illumination of laser beams with power densities higher than a critical value ($\sim 15 \text{ mW/cm}^2$ for a 630 nm laser), resulting in the growth of silver (Ag) nanoplates on the GaAs surface. The density and dimensions (including both thickness and edge length) of the resulting nanoplates can be readily tuned by controlling the growth time and laser power density. The as-grown Ag nanoplates on the substrates significantly enhance Raman signals of interesting molecules and serve as a new class of promising surface-enhanced Raman scattering substrates for sensitive chemical detection.

Introduction

Direct deposition of anisotropic metal nanostructures on solid substrates is attracting a great deal of attention due to potential applications in surface-enhanced Raman scattering (SERS),^{1–3} field emission for displays,⁴ metamaterials,⁵ superlenses,⁶ efficient photocatalysis,⁷ and photoelectrochemical cells for solar energy conversion and hydrogen evolution.^{8–11} The most straightforward strategies for growing anisotropic metal nanoparticles on substrates can be classified into two categories: (i) physical evaporation of metals on the substrates against appropriate templates,¹² and (ii) chemical synthesis of metal nanoparticles in solutions followed by deposition and/or assembly on the substrates.¹³ Although the former template-assisted physical deposition is, in principle, capable of generating nanostructures made of any metal on many kinds of substrates, the preparation of appropriate templates is nontrivial and the use of high-vacuum evaporation instruments results in high cost and time-consuming processing. In addition, the resulting metal nanoparticles are polycrystalline and have rough surfaces. The latter protocol based on chemical synthesis and postdeposition represents a cost-effective strategy since a number of solution-phase methodologies have been developed to successfully synthesize metal nanostructures with a wide range of well-defined shapes, such as spheres,^{14–19} cubes,^{20–28} tetrahedra,²⁹ octahedra or truncated octahedra,^{21,24–26,30–32} decahedra,^{32–34} tetrahedra,³⁵ rings/frames,³⁶ rods/wires/beams,^{28,37–45} stars,^{46–50} plates,^{36,51–60} boxes,^{20,61–63} and cages.^{27,61,62,64} These solution-phase syntheses are usually performed under ambient atmosphere and in the absence of templates. The as-synthesized metal nanoparticles, which are usually highly crystalline (e.g., single crystals for many nanoparticles), can be subsequently deposited on appropriate substrates through various techniques, such as spin-casting and Langmuir–Blodgett assembly/transferring.⁶⁵ The possible disadvantage of these chemical protocols is the use of surfactants that attach to the surfaces of the metal nanoparticles to guide their anisotropic growth as well as to prevent them from aggregating and sintering during synthesis. These surfactant layers may deteriorate the performance of the

metal nanoparticles in some applications. For instance, they may increase resistive barriers for charge transfer between the metals and semiconductors when the metal nanoparticles are deposited on semiconductor substrates for devices such as transistors and photoelectrochemical cells.⁶⁶ Most recently, direct galvanic reactions between semiconductor wafers and solutions of metal salts have been demonstrated to be capable of growing metal nanoparticles on semiconductor substrates without surfactant contamination.^{67,68} However, the morphologies of the nanoparticles in previous reports are irregular, making it difficult to tailor their properties.

We recently have developed an effective approach to grow high-quality Ag nanoplates on single-crystalline, highly doped n-type GaAs substrates through a simple galvanic reaction between pure aqueous solutions of AgNO_3 and pristine GaAs wafers.^{69–74} Although this strategy can be extended to grow other metal nanoplates on other n-type semiconductors (e.g., Pd nanoplates on n-GaAs, Ag nanoplates on n-Si), it fails to grow metal nanoplates on p-type semiconductor wafers. Our previous studies indicated that this failure is due to the shortage of surface electrons for the formation of nuclei, which are crucial to the subsequent growth of metal nanoplates. Herein, we report an effective means to increase the concentration of surface electrons in p-type semiconductor wafers by illuminating the wafers with light having photon energy higher than the semiconductor band gap. To demonstrate this strategy, Ag nanoplates have been successfully grown on p-GaAs substrates with quality similar to those grown in the dark on n-GaAs substrates. The sizes and density of the Ag nanoplates can be tuned by controlling the growth time and illumination power density. The resulting Ag nanoplates strongly enhance Raman signals of molecules attached to their surfaces.

Experimental Section

Growth of Ag Nanoplates. GaAs wafers doped with Zn at a concentration of $\sim 1 \times 10^{19} \text{ cm}^{-3}$ and with surfaces oriented along [100] were purchased from AXT (Fremont, CA). Each wafer was cut into $\sim 1 \text{ cm} \times 1 \text{ cm}$ square pieces along their cleavage planes (i.e., [011] and [011]) and were cleaned by immersing them in a 2% hydrofluoric acid (HF) aqueous

* To whom correspondence should be addressed, ygsun@anl.gov.

solution (Fisher) for 5 min. **Caution:** appropriate personal protective equipment is required to handle HF, which is highly corrosive toward tissues, bones in particular. The GaAs pieces were then thoroughly rinsed with deionized (DI) water followed by drying with N_2 flow. The cleaned wafers were then ready to react with an aqueous solution of 2 M $AgNO_3$ (Aldrich). In a typical synthesis, a droplet ($\sim 60 \mu L$) of $AgNO_3$ solution was delivered to the central area of the flat surface of a cleaned GaAs substrate with a micropipettor. A linearly polarized, red laser beam with a diameter of ~ 1 mm was then turned on to illuminate the wetted GaAs surface. The power density was controlled by rotating a polarizer between the laser and the GaAs substrate. The reaction was terminated by immersing the GaAs wafer in a large volume (~ 1 L) of water to remove excess $AgNO_3$. Finally, the wafer was thoroughly rinsed with DI water and dried with gentle N_2 flow.

Characterization with Electron Microscopy. A Quanta 400F (FEI) microscope operated at 20 kV under high vacuum mode was used to record the scanning electron microscopy (SEM) images of the as-grown samples. Samples for transmission electron microscopic (TEM) imaging and electron diffraction were prepared by following a standard milling procedure.⁷⁵ In a typical process, a sample was first cleaved into narrow slices (with widths around 3 mm) along the natural cleavage planes of single crystalline GaAs. These slices and some small pieces of GaAs wafers, which were used as references, were then bound to a holder with LOCTITE 495 superbond instant adhesive. These GaAs slices with Ag nanoplates were ground and polished to thicknesses of less than $10 \mu m$. The thinned samples were released from the holder by dissolving the adhesive in acetone. Each sample was placed on a 3 mm copper grid and ion milled to a thickness (<100 nm) that provides electron transparency. The entire ion milling process was carried out while the samples were cooled with liquid nitrogen to prevent the GaAs from becoming amorphous. All the TEM images and diffraction patterns were recorded on a JEOL 2100 transmission electron microscope operated at 200 kV.

Characterization with Synchrotron X-ray Diffraction. X-ray diffraction characterization was performed on a bending magnet beamline, 12-BM-B, at the Advanced Photon Source (APS) at Argonne National Laboratory. A 12-keV X-ray beam from an Si(111) monochromator with flux of 3.8×10^{10} photons/s was used to produce Bragg diffractions from Ag. In a typical measurement, a GaAs substrate covered with Ag nanoplates was mounted on a home-built motorized stage, which can be rotated and moved in three directions through computer control. Manipulating the stage aligned the Ag nanoplates so that the X-ray beam impinged on them at an incidence angle of about 10° with respect to the surface of the GaAs substrate. The X-ray beam was diffracted into many cones in space, as in X-ray powder diffraction. The diffracted signals were intercepted by an X-ray CCD camera (Mar165, pixel size of $79 \mu m$, $2 K \times 2 K$ array) that was placed perpendicular to the incident beam at a distance of 850 mm to the sample, resulting in a two-dimensional (2D) image with a series of concentric Debye rings. The 2D image data were processed with analysis software Fit2D (<http://www.esrf.eu/computing/scientific/FIT2D/>).

Characterization with Raman Spectroscopy. Raman spectra were measured on a Raman microscope (Renishaw, inVia) with excitation wavelength of 514 nm. A $50\times$ microscope objective was used to focus the laser excitation (0.6 mW) onto the samples as well as to collect the scattered light. In a typical sample, monolayers of thiophenol molecules were self-assembled on the surfaces of the Ag nanoparticles and GaAs

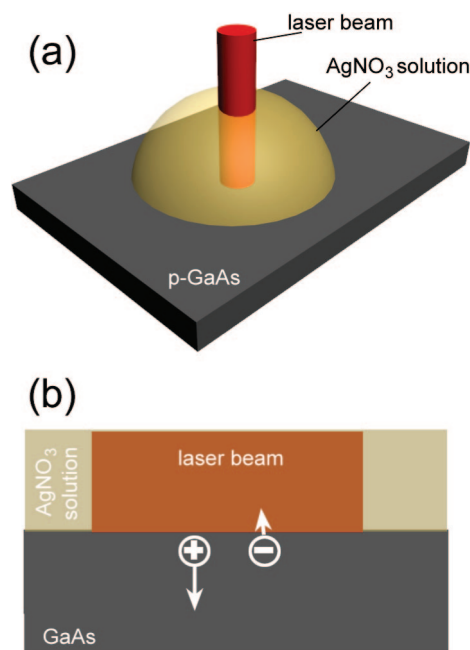


Figure 1. (a) Schematic illustration of the experimental setup for growth of Ag nanoplates on p-type GaAs substrates. (b) Cross-sectional diagram highlighting the migration of electrons and holes generated through photoillumination. \oplus and \ominus denote positive charges (i.e., holes) and electrons, respectively.

substrates by soaking the sample in a 5% ethanolic solution of thiophenol (Aldrich) for 60 min at room temperature. The sample was then thoroughly rinsed with ethanol, resulting in the removal of the physically adsorbed thiophenol molecules. Exposing the sample to a gentle N_2 flow dried its surface.

Results and Discussion

In a typical synthesis, a droplet of aqueous solution of $AgNO_3$ is delivered to the surface of a piece of p-GaAs wafer that has been cleaned by dipping in a 2% HF solution for 5 min. Part of the wetted surface is then illuminated with a 650 nm (1.9 eV) laser beam. Figure 1a shows a sketch of the experimental setup. When the laser is turned on for a certain period, Ag nanoplates are grown in the illuminated area. Because the photon energy of the laser is higher than the band gap of GaAs (1.42 eV), electrons are excited from the valence band of GaAs to its conduction band. The excited electrons migrate to the GaAs surface to facilitate the nucleation and growth of Ag nanoplates through reduction of Ag^+ ions, while the leftover holes in the valence band remain in the GaAs lattice (Figure 1b). After Ag nuclei with appropriate crystalline structures are formed in the illuminated region, they continue to grow into Ag nanoplates through reduction of Ag^+ by surface electrons supplied by the continuous laser illumination and/or by a hole injection process.^{70,73}

Figure 2 shows a series of SEM images of a sample prepared through the reaction between a $60 \mu L$ droplet of 2 M $AgNO_3$ solution and a p-GaAs wafer for 1 min under laser irradiation with a power density of 54.0 mW/cm^2 . The low-magnification image of Figure 2a shows clear contrast between the illuminated and dark areas, indicating that laser illumination significantly enhances the deposition of silver particles. High-magnification images (Figure 2b) reveal that the Ag particles densely deposited (with density of $\sim 3.9 \times 10^9 \text{ cm}^{-2}$) in the laser beam area have platelike geometries and flat surfaces. The thicknesses of the Ag nanoplates range from 30 to 50 nm (with an average of

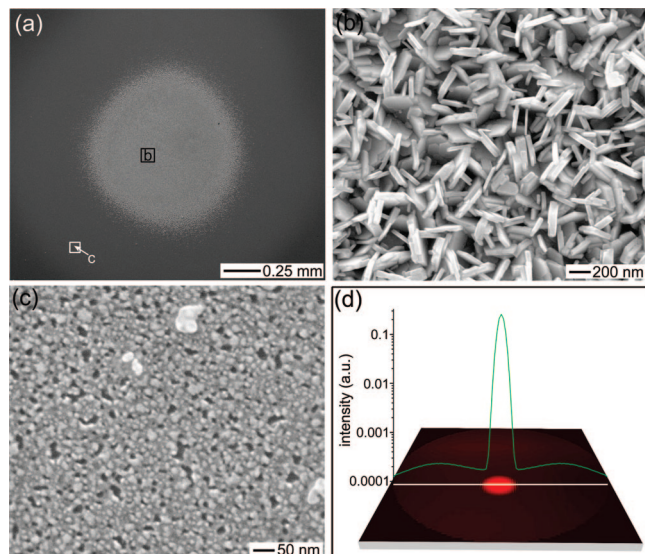


Figure 2. (a–c) SEM images of Ag nanostructures grown on a p-type GaAs wafer in contact with 2 M AgNO₃ solution, with a portion of the wetted area illuminated by a red laser beam with power density of 54.0 mW/cm² (as shown in Figure 1a). The frames of (b, c) correspond to the areas highlighted by the boxes labeled with corresponding letters in (a). Reaction conditions: temperature of ~22 °C; growth time of 1 min; volume of AgNO₃ solution of ~60 μ L. (d) Calculated two-dimensional and sectional (indicated by the green line) plots of the spatial distribution of light intensity over the GaAs surface and underneath a droplet of AgNO₃ solution. In the calculation, 70% of the incident laser power is scattered by the Ag nanoplates. The water droplet used in this calculation has a diameter of 8 mm and a height above the substrate of 2.5 mm. The laser beam has a diameter of 1 mm and is offset 1 mm from the center of the droplet. Laser intensity is shown on a logarithmic scale.

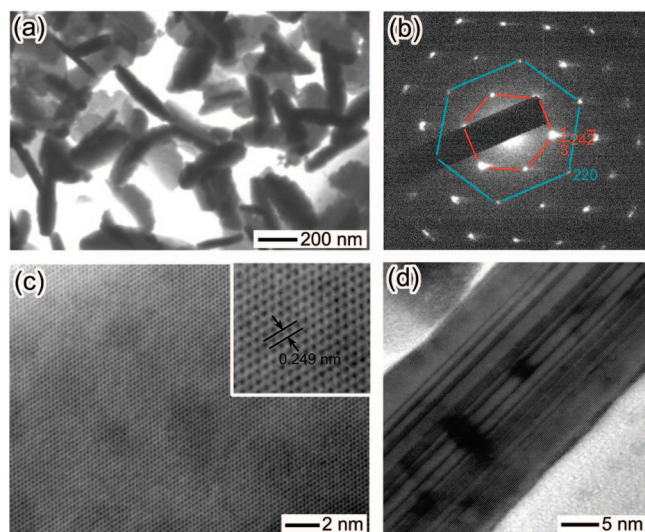


Figure 3. TEM images (a, c, d) and electron diffraction pattern (b) of the Ag nanoplates as shown in Figure 2.

~38 nm) and their edge lengths are ~300 nm. The Ag nanoplates protrude out of the surface of the GaAs substrate with random orientations.

A typical TEM image of these nanoplates is presented in Figure 3a, confirming their platelet morphologies. Aligning the electron beam perpendicular to the basal surfaces of an individual nanoplate produces a strong diffraction pattern with hexagonal symmetry (Figure 3b), indicating that the basal surfaces of the nanoplates are bounded by {111} facets. The set of diffracted spots marked with cyan lines corresponds to a

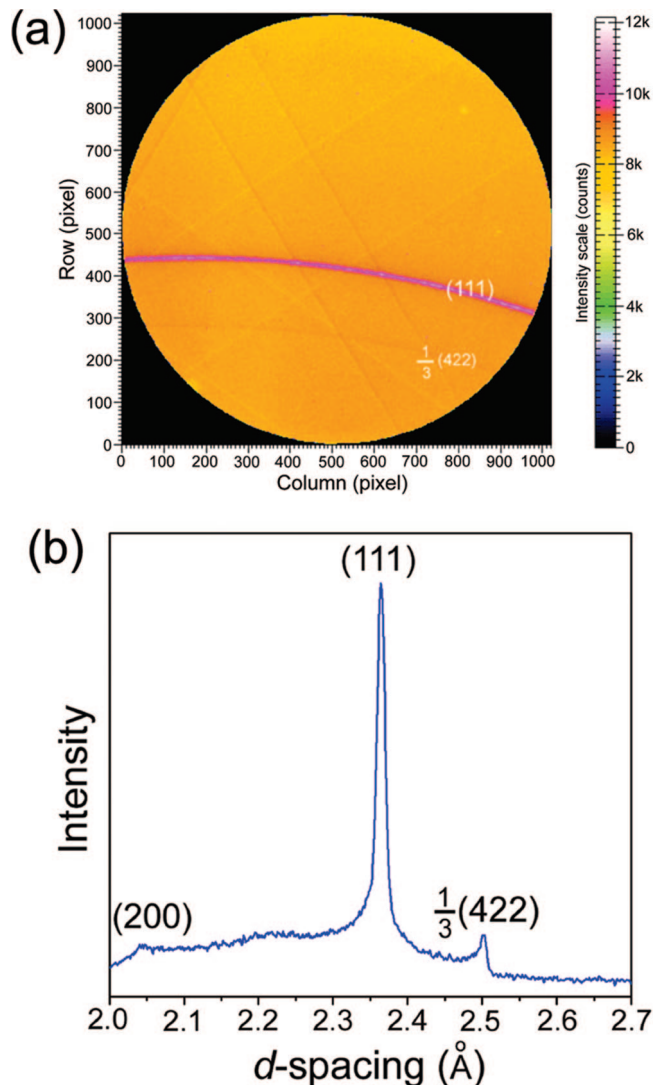


Figure 4. (a) X-ray diffraction pattern recorded by a CCD camera for the as-grown Ag nanoplates. The weak straight lines are attributed to the Kikuchi patterns of the GaAs substrate. (b) Plot of the diffracted X-ray intensity as a function of the calculated d spacing. The peaks are consistent with an fcc silver lattice.

lattice spacing of 1.44 Å and can be indexed to the {220} reflection of face-centered cubic (fcc) silver, while the inner set (marked with red lines), corresponding to a lattice spacing of 2.49 Å, originates from the (1/3){422} reflection that is normally forbidden by an fcc lattice. The strong (1/3){422} reflection is further confirmed by the high-resolution TEM (HRTEM) image (Figure 3c), which clearly shows continuous lattice fringes with periodicity of 2.49 Å. The appearance of the (1/3){422} reflection is ascribed to the formation of multiple (111) twin planes parallel to the basal surfaces of the nanoplates. Figure 3d shows a TEM image taken from the side of a nanoplate by aligning the electron beam parallel to the basal surfaces of the nanoplate, along the [110] zone axis. The image clearly shows the existence of twin boundaries parallel to the basal surfaces. These characteristic results indicate that each nanoplate fans out along the [110] direction with confinement of (111) twin planes during growth.

Crystal structures of the as-grown Ag nanoplates have been further studied with X-ray diffraction. Figure 4a shows a typical 2D diffraction pattern with concentric stripes, corresponding to the signals diffracted from different lattices. The uniformity in intensity of each stripe at different positions indicates that the

Ag nanoplates are oriented randomly without correlation to the orientation of the GaAs substrate. This 2D image can be converted into a conventional plot of X-ray intensity against d spacing, as shown in Figure 4b. Strong peaks centered at 2.364 and 2.496 Å agree well with the d spacing of {111} and (1/3){422} planes of Ag, respectively. The X-ray diffraction patterns are consistent with the electron diffraction patterns. The high ratio between the intensity of the (111) and (200) peaks is attributed to the platelet geometry of the Ag nanoplates with large {111} surfaces. These results are similar to those for Ag structures grown on highly doped n-GaAs wafers in the dark through reaction with a 2 M AgNO₃ solution for 6 min (see Figure 10F in ref 71). The similarities confirm that photoillumination of p-GaAs wafers enhances the density of surface electrons, enabling the nucleation of Ag nanoparticles on p-GaAs in the same way as on n-GaAs. The faster growth rate of the Ag nanoplates on the illuminated p-GaAs substrates indicates that the surface electrons generated from photoillumination also facilitate the growth of Ag nanoplates.

Areas of the p-GaAs substrate that are wetted with AgNO₃ solution and not directly illuminated with the laser beam are covered with a monolayer of small, irregular Ag particles with sizes of 10–20 nm (Figure 2c). The reaction of a p-GaAs wafer in the dark with a 2 M AgNO₃ solution for 1 min, on the other hand, results in the formation of only sparse particles with surface coverage of <1%. Formation of small Ag nanoparticles with high density is ascribed to scattering of the laser beam by the Ag nanoplates. The light scattering leads to low-intensity illumination of the whole wetted surface area (aside from the area directly illuminated by the laser beam). Figure 2d presents the calculated spatial distribution of light intensity over the wetted surface when 70% of the incident laser power is scattered by the Ag nanoplates, showing that the surface area away from the laser beam is illuminated by the scattered light. In the calculation, it is assumed that every point on the surface under the laser beam scatters light isotropically in all directions above the sample surface. A fraction of the light scattered into each direction will reflect off the water/air interface at the top of the droplet and return to the substrate. The optical power density on the surface due to scattering and reflection is calculated using standard ray-tracing techniques, in which angle- and polarization-dependent Fresnel relations are used to determine the reflection coefficient at the top of the droplet,⁷⁶ and it is assumed that light is scattered only once off the substrate. The calculation results are a weighted average of the optical power density due to scattering at each point within the Gaussian laser spot. The significant difference in morphologies of the Ag nanostructures grown in the area directly illuminated by the laser beam and those in the areas away from the laser beam indicates that the crystal structures of the nuclei and growth rate of the Ag nanoparticles are strongly dependent on the power density of light illumination, as discussed in detail below.

The dimensions of the Ag nanoplates can be easily tuned by controlling the growth time under constant light illumination. Figure 5 compares SEM images of Ag nanoplates grown for different times with the same reaction conditions as those for Figure 2. The edge lengths of the Ag nanoplates gradually increase with growth time up to 1 min, while their thicknesses remain essentially constant (Figures 5a, 5b, and 2b). The constant thickness during the growth indicates that each nanoplate may start with a nucleus that has multiple {111} twin planes and lateral dimensions similar to the thickness of the plate.⁶⁹ The multiply twinned structure induces the nucleus to grow by expanding its {111} surfaces, through continuous

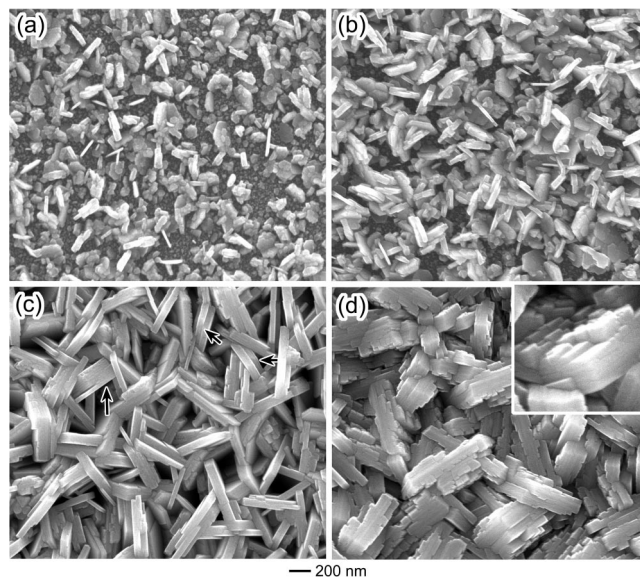


Figure 5. SEM images of Ag nanoplates grown on p-GaAs wafers for different times: (a) 30 s, (b) 45 s, (c) 2 min, and (d) 4 min. Other reaction conditions were the same as those for Figure 2b.

addition of Ag atoms to its high-index lateral surfaces, resulting in the formation of a plate. In addition to the nanoplates, many additional small nanoparticles with sizes less than 20 nm also exist on the GaAs surface, as can be clearly seen for the samples grown for short times (e.g., Figure 5a). The codeposition of the smaller particles is attributed to the progressive nucleation caused by excess surface electrons continuously provided by photoillumination. After the plates have grown for approximately 1 min, adjacent nanoplates with the same orientation start to overlap along their basal surfaces, leading to polymerization into oligomers, such as the dimers and trimers highlighted by the arrows in Figure 5c. Continued growth smooths the stepped edges of the oligomers and fuses them into thicker nanoplates whose thicknesses are approximately equal to the sum of the individual plate thicknesses before fusion (Figure 5c). The polymerization and fusion processes cease when the thick Ag nanoplates completely cover the GaAs substrates. Continued reaction deposits more Ag atoms on the basal (111) surfaces of the Ag nanoplates, forming additional layers of Ag platelets (Figure 5d), and causing the Ag nanoplates to become thicker. The inset of Figure 5d clearly shows that many flat Ag layers are deposited on the surface of the original large nanoplate. This overgrowth is not observed in the reaction of AgNO₃ solution with n-GaAs substrates, even though similar polymerization and fusion processes occur.⁷¹ The possible reason for this difference is that the high-density surface electrons generated by photoillumination of p-GaAs substrates flow to the surfaces of the Ag nanoplates, inducing nucleation and epitaxial overgrowth of Ag.

As indicated in Figure 2, the power density of incident light strongly influences the morphologies of the Ag nanostructures. This dependence offers control over the growth of Ag nanostructures on p-GaAs substrates by tuning the intensity of the incident laser beam. Figure 6 compares SEM images of samples grown for 2 min (i.e., the same as for Figure 5c) under different laser power densities. The results demonstrate that the quality of the Ag nanoplates formed under illumination with laser beams of 54.0 (Figure 5c), 31.2 (Figure 6a), and 16.4 mW/cm² (Figure 6b) are essentially the same. However, only irregular nanoplates with much lower density are formed when the power density of the laser beam decreases to 12.6 mW/cm² (Figure 6c),

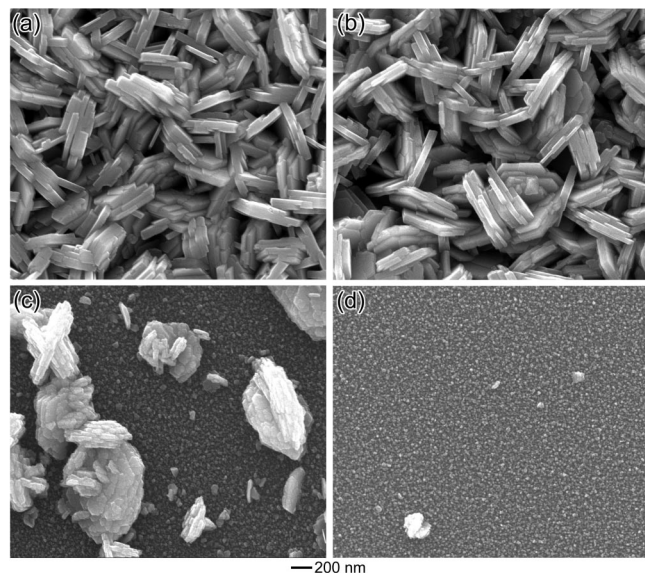


Figure 6. SEM image of Ag nanoparticles grown on p-GaAs wafers for 2 min under illumination by a laser beam with different power densities: (a) 31.2, (b) 16.4, (c) 12.6, and (d) 8.2 mW/cm². Other reaction conditions were the same as those for Figure 5c.

indicating that the growth of high-quality Ag nanoplates on the p-GaAs substrates requires a laser beam with power density higher than a critical value of about 15 mW/cm². There are almost no plates formed when the laser power density is less than ~ 8 mW/cm² (Figures 6d and 2c). Instead, only very small nanoparticles with sizes less than 20 nm are formed. These nanoparticles do not grow into larger ones even though the concentration of AgNO₃ is high enough to support hole injection.^{69,70} These results indicate that maintaining a relatively high laser power density is crucial to drive the growth of Ag nanoplates with quality comparable to those grown on n-GaAs substrates.

The morphological dependence of the Ag nanostructures on illumination power density is also confirmed when we examine the Ag nanostructures formed at different regions of an individual sample, such as the one shown in Figure 2. The power in the laser beam follows a Gaussian distribution, with a gradual decrease of power density from the center to the edge. Reactions in the areas outside of the contour line of the critical power density (i.e., ~ 15 mW/cm²) cannot effectively support the growth of high-quality Ag nanoplates. The variation of Ag nanostructures can be directly observed in optical images such as zones 1–4 in Figure 7a and the corresponding SEM images, such as Figure 2b, the left inset of Figure 7d, the right inset of Figure 7d, and Figure 2c, respectively.

Nanostructures made of noble metals such as Au and Ag have been extensively used to enhance Raman signals of molecules close to their surfaces, resulting in a sensitive detection protocol including single-molecule detection.^{77–79} Extensive theoretical and experimental studies have demonstrated that the most intense SERS is observed when the surface plasmon of metal nanoparticles is in resonance with the incident light.⁸⁰ Surface plasmon resonant frequencies of a metal nanoparticle are sensitive to its geometry, which also determines the spatial distribution of electromagnetic fields near the nanoparticle surfaces.⁸¹ In general, nanoparticles with sharp points and edges exhibit high electrical near fields adjacent to these sharp features, resulting in strong SERS effects.⁸² The as-grown Ag nanoplates on p-GaAs substrates have many sharp edges and corners, which make them promising as SERS substrates.

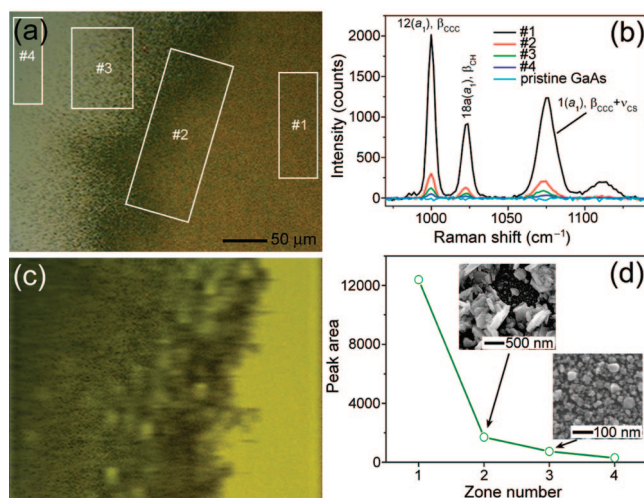


Figure 7. Raman scattering from self-assembled monolayers of thiophenol molecules deposited on a sample of Ag nanoplates on a GaAs surface. The measured areas are shown in the optical image (a). The representative SEM images for zones 1–4 are presented in Figure 2b, the left inset of Figure 7d, the right inset of Figure 7d, and Figure 2c, respectively. (b) Averaged Raman spectra recorded in different zones, normalized against their baselines. The vibrational assignments for the major peaks are marked in the figure, and the letters in parentheses represent the vibrational symmetry. γ , β , and ν denote the out-of-plane bending, in-plane bending, and in-plane stretching modes, respectively. (c) Overlay of peak height at ~ 1000 cm⁻¹ over the area shown in (a). Brighter yellow indicates higher Raman intensity. (d) Comparison of the integrated areas of the 1000 cm⁻¹ peak recorded in different zones.

Figure 7b presents Raman spectra of self-assembled monolayers of thiophenol molecules chemically bonded to the surfaces of the Ag nanoplates and the GaAs substrates, for the different zones marked in Figure 7a. These signals are averaged over the excitation laser spot, which has a diameter of approximate 1.2 μ m. The characteristic peaks are consistent with the vibration frequencies of the thiophenol molecules.⁸³ The significant variation in intensity of the Raman peaks recorded in different zones indicates that the assemblies of Ag nanostructures with different morphologies exhibit different enhancement factors. This is highlighted in Figure 7c, which shows a spatial map of the height of the peak at 1000 cm⁻¹. The intensity in the center of the growth area (zone 1) is much higher than that in the edge areas (zones 2 and 3) and in the area that was not directly illuminated during growth (zone 4). The decrease of Raman intensity is attributed to the decreased density of Ag nanoplates from the center of the illuminated region to the dark region. Figure 7d quantitatively compares the Raman intensity in different areas by integrating the area of the peak at 1000 cm⁻¹ against its baseline. The average Raman signal in zone 1 (for the Ag nanoplates as shown in Figure 2b) is ~ 42 times higher than that in zone 4 (for the small Ag nanoparticles as shown in Figure 2c). On the other hand, the surface area of the Ag nanoplates in zone 1 is only ~ 3.5 times of that in zone 4. (In the estimation of surface areas of the Ag nanoplates, we approximate the nanoplates as circular disks with diameters equal to the measured edge lengths and the small Ag nanoparticles as hemispheres with diameter of 15 nm.) This means that the assembly of Ag nanoplates on the p-GaAs substrates exhibits a SERS enhancement factor at least 12 times higher than the small, irregular Ag nanoparticles. Due to the spatial selectivity of laser-driven growth, substrates with patterned patches of Ag nanoplates could readily be prepared for high-throughput,

sensitive chemical detection, by spatially controlling laser illumination during growth.

Conclusion

Ag nanoplates have been successfully grown on highly doped p-type GaAs wafers through direct reaction between the wafers themselves and aqueous solutions of AgNO₃ under laser illumination. The density and dimensions of the Ag nanoplates can be easily tuned by adjusting the power density of the laser beam and the growth time. Optimizing the growth conditions provides the potential to directly deposit Ag nanoplates on p-GaAs wafers with controlled quality comparable to that of nanoplates grown on n-GaAs wafers. The selective deposition in the illuminated areas makes it possible to pattern semiconductor substrates with Ag nanoplates in arbitrary arrangements. In combination with the excellent SERS performance of the Ag nanoplates, this may enable the low-cost fabrication of chips for high-throughput chemical sensing. Coupling the optical and electronic properties of the Ag nanoplates and the p-GaAs substrates may lead to additional novel phenomena. For example, the Ag nanoplates may be able to efficiently extract electrons from the p-GaAs substrate to induce catalytic reactions that are sensitive to {111} Ag surfaces when the composite materials are excited with light.⁷

Acknowledgment. The submitted manuscript has been created by UChicago Argonne, LLC, Operator of Argonne National Laboratory ("Argonne"). Argonne, a U.S. Department of Energy Office of Science laboratory, is operated under Contract No. DE-AC02-06CH11357. Use of the Center for Nanoscale Materials, the Electron Microscopy Center for Materials Research, and the Advanced Photon Source at Argonne was supported by the U.S. Department of Energy, Office of Science, Office of Basic Energy Sciences, under Contract No. DE-AC02-06CH11357. Characterizations were also carried out by partially using the Center for Microanalysis of Materials Facilities in Frederick Seitz Materials Research Laboratory, University of Illinois, which is partially supported by the U.S. Department of Energy under Grant No. DEFG02-91-ER45439. Y.S. thanks Drs. Changhui Lei and Hanfei Yan for the help with TEM and X-ray diffraction characterization.

References and Notes

- (1) *Chem. Soc. Rev.* **2008**, 37, special issue.
- (2) Brown, R. J. C.; Milton, M. J. T. *J. Raman Spectrosc.* **2008**, 39, 1313.
- (3) Dieringer, J. A.; McFarland, A. D.; Shah, N. C.; Stuart, D. A.; Whitney, A. V.; Yonzon, C. R.; Young, M. A.; Zhang, X.; Van Duyne, R. P. *Faraday Discuss.* **2006**, 132, 9.
- (4) Kim, C.; Gu, W.; Briceno, M.; Robertson, I. M.; Choi, H.; Kim, K. *Adv. Mater.* **2008**, 20, 1859.
- (5) Yao, J.; Liu, Z.; Liu, Y.; Wang, Y.; Sun, C.; Bartal, G.; Stacy, A. M.; Zhang, X. *Science* **2008**, 321, 930.
- (6) Fang, N.; Lee, H.; Sun, C.; Zhang, X. *Science* **2005**, 308, 534.
- (7) Costi, R.; Saunders, A. E.; Elmaleh, E.; Salant, A.; Banin, U. *Nano Lett.* **2008**, 8, 637.
- (8) Lewis, N. S. *J. Electroanal. Chem.* **2001**, 508, 1.
- (9) Lombardi, I.; Marchionna, S.; Zangari, G.; Pizzini, S. *Langmuir* **2007**, 23, 12413.
- (10) Nakato, Y.; Ueda, K.; Yano, H.; Tsubomura, H. *J. Phys. Chem.* **1988**, 92, 2316.
- (11) Waki, I.; Cohen, D.; Lal, R.; Mishra, U.; DenBaars, S. P.; Nakamura, S. *Appl. Phys. Lett.* **2007**, 91, 093519.
- (12) Haynes, C. L.; Van Duyne, R. P. *J. Phys. Chem. B* **2001**, 105, 5599.
- (13) Cui, Y.; Bjork, M. T.; Liddle, J. A.; Sonnichsen, C.; Boussert, B.; Alivisatos, A. P. *Nano Lett.* **2004**, 4, 1093.
- (14) Kim, M. H.; Lu, X.; Wiley, B.; Lee, E. P.; Xia, Y. *J. Phys. Chem. C* **2008**, 112, 7872.
- (15) Wang, C.; Daimon, H.; Onodera, T.; Koda, T.; Sun, S. *Angew. Chem., Int. Ed.* **2008**, 47, 3588.
- (16) Ghosh, D.; Chen, S. *J. Mater. Chem.* **2008**, 18, 755.
- (17) Yin, Y.; Erdonmez, C. K.; Aloni, S.; Alivisatos, A. P. *J. Am. Chem. Soc.* **2006**, 128, 12671.
- (18) Wang, Y.; Yang, H. *Chem. Commun.* **2006**, 2545.
- (19) Tang, Y.; Ouyang, M. *Nat. Mater.* **2007**, 6, 754.
- (20) Sun, Y.; Xia, Y. *Science* **2002**, 298, 2176.
- (21) Kim, F.; Connor, S.; Song, H.; Kuykendall, T.; Yang, P. *Angew. Chem., Int. Ed.* **2004**, 43, 3673.
- (22) Yu, D.; Yam, V. W.-W. *J. Am. Chem. Soc.* **2004**, 126, 13200.
- (23) Xiong, Y.; Chen, J.; Wiley, B.; Xia, Y.; Yin, Y.; Li, Z.-Y. *Nano Lett.* **2005**, 5, 1237.
- (24) Song, H.; Kim, F.; Connor, S.; Somorjai, G. A.; Yang, P. *J. Phys. Chem. B* **2005**, 109, 188.
- (25) Tao, A.; Sinsermsuksakul, P.; Yang, P. *Angew. Chem., Int. Ed.* **2006**, 45, 4597.
- (26) Seo, D.; Park, J. C.; Song, H. *J. Am. Chem. Soc.* **2006**, 128, 14863.
- (27) Skrabalak, S. E.; Au, L.; Li, X.; Xia, Y. *Nat. Protoc.* **2007**, 2, 2182.
- (28) Wiley, B.; Sun, Y.; Xia, Y. *Langmuir* **2005**, 21, 8077.
- (29) Zhou, J.; An, J.; Tang, B.; Xu, S.; Cao, Y.; Zhao, B.; Xu, W.; Chang, J.; Lombardi, J. R. *Langmuir* **2008**, 24, 10407.
- (30) Zhang, J.; Gao, Y.; Alvarez-Puebla, R. A.; Buriak, J. M.; Fenniri, H. *Adv. Mater.* **2006**, 18, 3233.
- (31) Li, C.; Shuford, K. L.; Park, Q.-H.; Cai, W.; Li, Y.; Lee, E. J.; Cho, S. O. *Angew. Chem., Int. Ed.* **2007**, 46, 3264.
- (32) Lim, B.; Xiong, Y.; Xia, Y. *Angew. Chem., Int. Ed.* **2007**, 46, 9279.
- (33) Sanchez-Iglesias, A.; Pastoriza-Santos, I.; Perez-Juste, J.; Rodriguez-Gonzalez, B.; de Abajo, F. J. G.; Liz-Marzan, L. M. *Adv. Mater.* **2006**, 18, 2529.
- (34) Petrobon, B.; Kitaev, V. *Chem. Mater.* **2008**, 20, 5186.
- (35) Tian, N.; Zhou, Z.-Y.; Sun, S.-G.; Ding, Y.; Wang, Z. L. *Science* **2007**, 316, 732.
- (36) Sun, Y.; Xia, Y. *Adv. Mater.* **2003**, 15, 695.
- (37) Sun, Y.; Mayers, B.; Herricks, T.; Xia, Y. *Nano Lett.* **2003**, 3, 955.
- (38) Sun, Y.; Xia, Y. *Adv. Mater.* **2002**, 14, 833.
- (39) Jana, N. R.; Gearheart, L.; Murphy, C. J. *Adv. Mater.* **2001**, 13, 1389.
- (40) Murphy, C. J.; Jana, N. R. *Adv. Mater.* **2002**, 14, 80.
- (41) Chen, J.; Herricks, T.; Geissler, M.; Xia, Y. *J. Am. Chem. Soc.* **2004**, 126, 10854.
- (42) Xiong, Y.; Cai, H.; Wiley, B. J.; Wang, J.; Kim, M. J.; Xia, Y. *J. Am. Chem. Soc.* **2007**, 129, 3665.
- (43) Wiley, B. J.; Chen, Y.; McLellan, J. M.; Xiong, Y.; Li, Z.-Y.; Ginger, D.; Xia, Y. *Nano Lett.* **2007**, 7, 1032.
- (44) Kim, F.; Song, J. H.; Yang, P. *J. Am. Chem. Soc.* **2002**, 124, 14316.
- (45) Kim, F.; Sohn, K.; Wu, J.; Huang, J. *J. Am. Chem. Soc.* **2008**, 130, 14442.
- (46) Maksimuk, S.; Teng, X.; Yang, H. *J. Phys. Chem. C* **2007**, 111, 14312.
- (47) Chen, S.; Wang, Z. L.; Ballato, J.; Foulger, S. H.; Carroll, D. L. *J. Am. Chem. Soc.* **2003**, 125, 16186.
- (48) Hao, E.; Bailey, R. C.; Schatz, G. C.; Hupp, J. T.; Li, S. *Nano Lett.* **2004**, 4, 327.
- (49) Teng, X.; Yang, H. *Nano Lett.* **2005**, 5, 885.
- (50) Chen, J.; Herricks, T.; Xia, Y. *Angew. Chem., Int. Ed.* **2005**, 44, 2589.
- (51) Sun, Y.; Mayers, B.; Xia, Y. *Nano Lett.* **2003**, 3, 675.
- (52) Jin, R.; Cao, Y. C.; Hao, E.; Metraux, G. S.; Schatz, G. C.; Mirkin, C. A. *Nature (London)* **2003**, 425, 487.
- (53) Chen, S.; Carroll, D. L. *Nano Lett.* **2002**, 2, 1003.
- (54) Jin, R.; Cao, Y. C.; Mirkin, C. A.; Kelly, K. L.; Schatz, G. C.; Zheng, J. G. *Science* **2001**, 294, 1901.
- (55) Pastoriza-Santos, I.; Liz-Marzan, L. M. *Nano Lett.* **2002**, 2, 903.
- (56) Shankar, S. S.; Rai, A.; Ankamwar, B.; Singh, A.; Ahmad, A.; Sastry, M. *Nat. Mater.* **2004**, 3, 482.
- (57) Sun, X.; Dong, S.; Wang, E. *Angew. Chem., Int. Ed.* **2004**, 43, 6360.
- (58) Chen, S.; Fan, Z.; Carroll, D. L. *J. Phys. Chem. B* **2002**, 106, 10777.
- (59) Xiong, Y.; McLellan, J. M.; Chen, J.; Yin, Y.; Li, Z.-Y.; Xia, Y. *J. Am. Chem. Soc.* **2005**, 127, 17118.
- (60) Washio, I.; Xiong, Y.; Yin, Y.; Xia, Y. *Adv. Mater.* **2006**, 18, 1745.
- (61) Sun, Y.; Xia, Y. *J. Am. Chem. Soc.* **2004**, 126, 3892.
- (62) Sun, Y.; Xia, Y. *Nano Lett.* **2003**, 3, 1569.
- (63) Sun, Y.; Mayers, B.; Xia, Y. *Adv. Mater.* **2003**, 15, 641.
- (64) Skrabalak, S. E.; Chen, J.; Sun, Y.; Lu, X.; Au, L.; Cobley, C. M.; Xia, Y. *Acc. Chem. Res.* **2008**, 41, 1587.
- (65) Tao, A.; Kim, F.; Hess, C.; Goldberger, J.; He, R.; Sun, Y.; Xia, Y.; Yang, P. *Nano Lett.* **2003**, 3, 1229.
- (66) Wu, Y.; Li, Y.; Ong, B. S. *J. Am. Chem. Soc.* **2006**, 128, 4202.
- (67) Nezhad, M. R. H.; Aizawa, M.; Porter, L. A., Jr.; Ribbe, A. E.; Buriak, J. M. *Small* **2005**, 1, 1076.

- (68) Aizawa, M.; Cooper, A. M.; Malac, M.; Buriak, J. M. *Nano Lett.* **2005**, 5, 815.
- (69) Sun, Y. *Chem. Mater.* **2007**, 19, 5845.
- (70) Sun, Y.; Wiederrecht, G. P. *Small* **2007**, 3, 1964.
- (71) Sun, Y.; Yan, H.; Wiederrecht, G. P. *J. Phys. Chem. C* **2008**, 112, 8928.
- (72) Sun, Y.; Yan, H.; Wu, X. *Appl. Phys. Lett.* **2008**, 92, 183109.
- (73) Sun, Y.; Lei, C.; Gosztola, D.; Haasch, R. *Langmuir* **2008**, 24, 11928.
- (74) Sun, Y.; Qiao, R. *Nano Res.* **2008**, 1, 292.
- (75) Lei, C. H. *Thin Solid Films* **2007**, 515, 3584.
- (76) Hecht, E. *Optics*, 4th ed.; Addison Wesley: Reading, MA, 2001.
- (77) Qian, X.-M.; Nie, S. M. *Chem. Soc. Rev.* **2008**, 37, 912.
- (78) Dieringer, J. A.; Lettan, R. B.; Scheidt, K. A.; Van Duyne, R. P. *J. Am. Chem. Soc.* **2007**, 129, 16249.
- (79) Camden, J. P.; Dieringer, J. A.; Wang, Y.; J., M. D.; Marks, L. D.; Schatz, G. C.; Van Duyne, R. P. *J. Am. Chem. Soc.* **2008**, 130, 12616.
- (80) Emory, S. R.; Haskins, W. E.; Nie, S. *J. Am. Chem. Soc.* **1998**, 120, 8009.
- (81) Kelly, K. L.; Coronado, E.; Zhao, L. L.; Schatz, G. C. *J. Phys. Chem. B* **2003**, 107, 668.
- (82) Yang, Y.; Matsubara, S.; Xiong, L.; Hayakawa, T.; Nogami, M. *J. Phys. Chem. C* **2007**, 111, 9095.
- (83) Joo, T. H.; Kim, M. S.; Kim, K. *J. Raman Spectrosc.* **1987**, 18, 57.

JP900638M